CHEMISTRY OF MATERIALS

ARTICLE

pubs.acs.org/cm

Colloidal Polymerization of Polymer-Coated Ferromagnetic Cobalt Nanoparticles into Pt-Co_3O_4 Nanowires

Pei Yuin Keng,[†] Mathew M. Bull,[†] In-Bo Shim,[‡] Kenneth G. Nebesny,[†] Neal R. Armstrong,[†] Younghun Sung,[§] Kookheon Char,[§] and Jeffrey Pyun*[,†,§]

[†]Department of Chemistry, University of Arizona, Tucson, Arizona 85721, United States

[‡]Department of Nano and Electronic Physics, Kookmin University, Seoul, Korea, 136-702

[§]World Class University Program for Chemical Convergence for Energy & Environment, Department of Chemical & Biological Engineering, Seoul National University, Seoul 151-744, Korea

Supporting Information

ABSTRACT: In this report, functional one-dimensional (1-D) Pt-Co_3O_4 heterostructures with enhanced electrochemical properties were synthesized via colloidal polymerization of polymer-coated ferromagnetic cobalt nanoparticles (PS-CoNPs). Colloidal polymerization of dipolar nanoparticles into hollow metal−semiconductor nanowires was achieved via a consecutive galvanic replacement reaction between Co^0 and Pt^{2+} precursors, followed by a nanoscale Kirkendall oxidation reaction and a calcination treatment. X-ray diffraction (XRD), transmission electron microscopy (TEM), high-angle annular dark field scanning TEM (HAADF-STEM), and field-emission scanning electron microscopy (FESEM) revealed the structural and morphological evolution of the hollow cobalt oxide nanowires (D = 40 nm) with platinum nanoparticles (PtNPs; $D \sim 2$ nm) entrapped within the growing oxide shell. Various calcination conditions were investigated via X-ray photoelectron spectroscopy (XPS) to obtain the optimal surface composition of the metallic Pt and semiconducting Co_3O_4 phases. Cyclic voltammetry of the 1-D Pt-Co_3O_4 heterostructures demonstrated a sevenfold enhancement in specific capacitance in comparison to the pristine Co_3O_4 nanowires. Preliminary results also showed that the calcined 1-D Pt-Co_3O_4 heterostructures catalytically hydrogenate methyl orange, and the rates of the hydrogenation were dependent on surface composition.

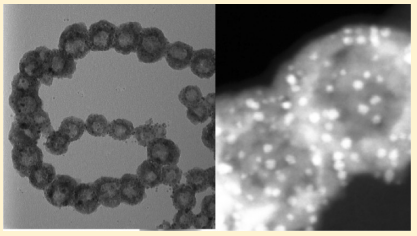

KEYWORDS: colloids, hybrid inorganic/organic materials, magnetic materials

INTRODUCTION

Recent advances in synthetic nanoscience have enabled progress in the development of novel hybrid nanoparticles consisting of discrete domains of disparate inorganic components.[1,2] Heterostructured nanocrystals with a high degree of morphological complexity and functionality have been observed to exhibit synergistic properties arising from the control of colloid size, morphology, and interfacial connectivity. Specifically, multicomponent metal−semiconductor nanostructures with controlled composition and morphology have been investigated as a route to direct charge transfer processes over nanoscopic length scales.[3−11]

A number of elegant approaches have been reported for the synthesis of symmetric core−shell hybrid nanoparticles (NPs), asymmetric heterodimers, hybrid nanorods, and nanowires consisting of metal, semiconductor, magnetic, and oxide materials.[1,2] Seminal work on the preparation of hybrid nanomaterials composed of core−shell cadmium selenide nanocrystals with higher band gap overcoats of zinc sulfide (ZnS)[12] and cadmium sulfide (CdS)[13] NP shells demonstrated the ability both to enhance the photoluminescence properties and increase the population of photogenerated charge carriers in CdSe cores. Hybrid nanoparticles composed of metal oxide colloidal cores (TiO_2, ZnO) with a metallic shell (Au, Pt, Cu) have also shown improved photocatalytic activity due to efficient charge separation at the nanoscopic metal−semiconductor oxide junction.[14−17]

In addition to the synthesis of symmetrical core−shell hybrid nanoparticles, the preparation of complex asymmetric heterostructures with diverse architectures has also garnered significant research interest. The synthesis of asymmetric heterodimers[18−22] composed of two or more chemically different crystalline domains was first demonstrated by Xu et al.[23] for the preparation of CdS/iron−platinum (FePt) heterodimeric nanoparticles. Notably, Sun, Hyeon, Teranishi, Prasad and co-workers further diversified the scope of synthetic methods toward the preparation of various well-defined heterostructures composed of colloidal metals, semiconductors, and metal oxides within a single nanomaterial.[18,24−26] Moreover, Banin et al.[9,10,27] and Cozzoli et al.[28] have also elegantly demonstrated selective growth of metal tips on semiconductor nanorods[29−32] in the preparation of platinum (Pt) functional

Received: August 12, 2010
Revised: December 16, 2010
Published: February 02, 2011

CdSe[33] and PtCo−CdSe nanorods,[34] which showed enhanced photocatalytic activity. In addition to heterostructured nanorods, Talapin and Mokari have also demonstrated the synthesis of well-defined lead sulfide (PbS)[35] and CdSe[10] nanowires decorated with gold (Au) nanocrystals. These one-dimensional (1-D) heterostructures are advantageous because the nanowire morphology provided directional electron transport in addition to enhanced charge separation at the metal−semiconductor interface.[7,8,33,36−39]

While significant progress has been reported for the preparation of n-type semiconductor (CdSe, TiO_2) hybrid nanomaterials for (photo)electrochemical devices, the investigation of p-type metal oxide semiconductors as potential heterostructured electrodes remains largely unexplored.[7,40−42] In particular, cobalt cobaltite (Co_3O_4), a p-type semiconductor oxide, has been investigated as electrodes for Li batteries,[42−44] supercapacitors,[45,46] (photo)-electrocatalysts for water splitting,[47−51] CO oxidation catalysts[52] and in electrochromic devices.[53,54] However, Co_3O_4 suffers from inherently high electrical resistance, moderate electrocatalytic activity, and high irreversible capacity in Li-ion batteries.[55−57] The incorporation of dopants into Co_3O_4 materials has been explored as a route to improve electrical conductivity and electrochemical activity of these cobalt oxides.[50,51,57,58]

The preparation of well-defined heterostructures composed of noble metals and Co_3O_4 nanomaterials has recently been explored. In particular, nanocomposites composed of Au nanoparticle inclusions within Co_3O_4 nanowires and nanocubes[44,56] have been reported to exhibit enhanced electrochemical activity in Li batteries and fuel cells relative to the pristine Co_3O_4 nanomaterials. The inclusion of noble metals into Co_3O_4 nanomaterials was observed to increase the electrical conductivity and charge transport of electrodes used for electrochemical devices, while decreasing the overall cell polarization.[56] While these reports demonstrate the advantages of preparing heterostructured Co_3O_4 nanomaterials, the development of versatile synthetic methods to prepare well-defined noble metal-Co_3O_4 nanocomposites remains an important challenge. We recently reported on the use of *colloidal polymerization* to prepare semiconducting cobalt oxide nanowires. In this process, dipolar cobalt nanoparticles were employed as "colloidal monomers" in a manner analogous to step-growth polymerization, which enabled the synthesis of hierarchically ordered 1-D cobalt oxide nanowires and heterostructures. We further utilized this method to prepare cobalt oxide nanowires with AuNP inclusions (Au−Co_3O_4) via colloidal polymerization of dipolar gold−cobalt core−shell nanoparticles (Au-CoNPs) as colloidal monomers.[59] These Au−Co_3O_4 heterostructured nanowires exhibited enhanced electrochemical activities relative to the Co_3O_4 control nanomaterials, as the presence of the AuNPs core reinforced cobalt oxide phases and afforded a higher number of electroactive sites.

Herein, we demonstrated the synthesis of 1-D Pt-Co_3O_4 heterostructures via a *colloidal polymerization*.[60] In this report, we demonstrate the ability to modify the exterior of cobalt oxide nanowires with platinum nanoparticle inclusions via consecutive galvanic exchange and Kirkendall-type oxidation reactions.[61−65] The galvanic exchange reactions have been exploited for the preparation of bimetallic core−shell, alloy, and hollow heterostructures of noble metals such as Pt, Au, and Pd.[61,62,66−68] Notably, Bai et al.[69] diversified this versatile methodology utilizing cobalt nanoparticles as sacrificial structure directing agents to prepare various metallic (Au, Pt, Pd) hollow nanospheres,[66,69−72] nanotubes, and nanowires.[67,68,73−76] Alternatively, a wide range of well-defined hollow nanocrystals were synthesized through oxidation, sulfidation, and nitridation of metallic nanoparticles.[64,65,77] The hollowing effect is a classical phenomenon known as the Kirkendall effect,[63] which refers to the nonuniform diffusion of the coupled species (e.g., O_2 and Co^0) leading to the coalescence of voids into a single hollow core. On the basis of these principles, we have expanded the scope for colloidal polymerization by the combination of both the galvanic exchange and the nanoscale Kirkendall-type reactions into 1-D Pt-Co_3O_4 heterostructures. While a number of heterostructured nanocrystals based on Pt have been developed, neither the preparation nor the electrochemical characterization of Pt−cobalt oxide based heterostructured nanomaterials using well-defined dipolar colloidal precursors has been conducted.

In the current colloidal polymerization methodology, the galvanic exchange reaction resulted in heterostructured chains with a PtNP shell and a partially exchanged Co core that were capped with polystyrene ligands (PtNP-CoNP chains) The Pt decorated nanoparticles were then oxidized to afford nanowires with hollow inclusions and a nanocomposite shell of PtNPs and Co_3O_4 (hereafter referred to as Pt-Co_3O_4 nanowires). Pt-Co_3O_4 nanowires prepared via *colloidal polymerization* were observed to exhibit sevenfold enhancement in specific capacitance relative to the hollow Co_3O_4 nanowires, as determined from electrochemical characterization. The unique combination of these chemical transformations could serve as a versatile platform to access various 1-D nanostructures with different properties, crystal structures, and morphologies with improved (photo)electrochemical properties.

RESULTS AND DISCUSSION

Polystyrene-coated ferromagnetic cobalt nanoparticles (PS-CoNPs) that were utilized as structure directing agents in the present report were prepared via the thermolysis of dicobalt octacarbonyl ($Co_2(CO)_8$) in the presence of the carboxylic acid end-functional polystyrene surfactants (PS-COOH), as reported elsewhere.[78] The synthesis of Pt NP (nanocrystallites, $D \sim 2$ nm) decorated cobalt nanoparticles chains was conducted by the addition of $Pt(acac)_2$ dissolved in dichlorobenzene (DCB) into a deaerated dispersion of the PS-CoNPs under argon at 175 °C for 10 h. The large electrochemical potential difference between Co^0 and Pt^{2+} (standard potential for $Co/Co^{2+}//Pt^{2+}/Pt = +1.46$ V vs SHE) drove the reduction of Pt^{2+} salts to Pt^0 colloids while oxidizing the CoNP core to Co^{2+} ions during the galvanic replacement reaction.[79] Consequently, Pt atoms selectively nucleated onto the outer surfaces of the PS-CoNPs chains in dichlorobenzene solution at zero field conditions (i.e., in the absence of an external magnetic field) (Scheme 1). As a result, Pt NPs grew and eventually formed a thin shell around the preorganized ferromagnetic cobalt nanoparticle chains, stringing individual magnetic PS-CoNPs into interconnected nanowires spanning on average 260 ± 88 nm in length.

The morphological evolution of the PS-CoNPs (D = 30 ± 3 nm) was monitored using TEM before and after transmetalation reactions with $Pt(acac)_2$. TEM of solution deposited samples imaged PS-CoNPs precursors as discrete, dark, solid nanoparticles separated by an outer polystyrene shell (Figure 1a). After 10 h of the galvanic exchange reaction with $Pt(acac)_2$, the formation of interconnected nanowires was observed with an increase in the overall diameter from 30 to 35 nm, while the inner diameter of the Co core decreased to 23 nm. The reduction in the Co core

Scheme 1. Preparation of Pt-Co_3O_4 Nanowires by Colloidal Polymerization of Ferromagnetic Cobalt Nanoparticles

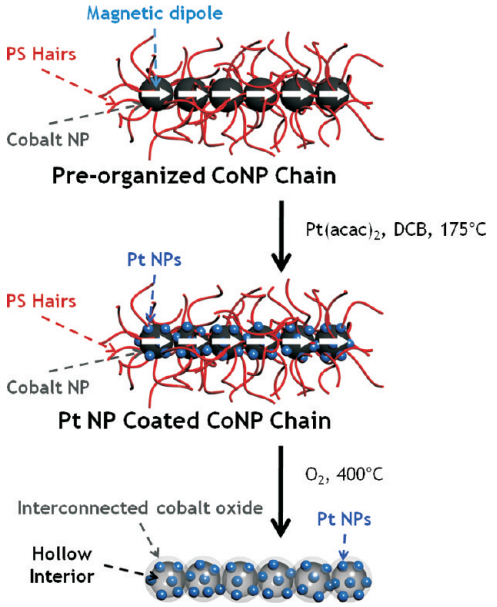

diameter was consistent with the mechanism of the galvanic exchange reaction, which was analogous to an electrochemical cell model of galvanic corrosion.[61] HRTEM images (Figure 1b) confirmed the formation of Pt NPs ($D \approx 2$ nm) on the periphery of the self-assembled PS-CoNPs chains. Additionally, high-angle annular dark field scanning TEM (HAADF-STEM) imaging was utilized to unambiguously confirm the formation of Pt NPs, which appeared as bright dots sprinkled on the outer corona of the lower contrast PS-CoNPs chains (Figure 1f). Furthermore, bright field STEM imaging confirmed that the growth of Pt NPs was confined to the exterior of the PS-CoNPs chains, which was consistent with the mechanism of the galvanic exchange reaction. Determination of the exact composition and chemical bonding of the Pt-Co interface is challenging to unambiguously ascertain due to the potential formation of metallic Pt-Co alloys, oxides, and other mixed phases at the interface that cannot be readily resolved via specotroscopic or scattering methods. We presume based on the morphology of Pt-Co heterostructures via TEM and FE-SEM (Figures 1 and 2) that the majority of PtNP inclusions are directly bound to CoNP cores. Futhermore, rigorous purification of Pt-Co heterostructure materials conducted by magnetic isolation and centrifugation did not increase the yield of free PtNPs nor change the morphology of isolated nanowires. However, given the high temperatures utilized in the PtNP galvanic deposition reaction, thermolysis of the $Pt(acac)_2$ could result in a small fraction of unbound PtNPs, as suggested by the diffuse morphology of Pt inclusions around CoNPs as observed in HAADF-STEM imaging (Figure 1f).

Kinetic studies on the transformations of discrete PS-CoNPs into Pt NP coated cobalt chains were analyzed via UV−vis spectroscopy by measuring the consumption of Pt^{2+} salts (see Supporting Information Figure S-1). A progressive reduction in the absorbance of $Pt(acac)_2$ complexes at 343 nm was observed within 5 h, confirming the consumption of Pt^{2+} salts in the presence of Co^0 nanoparticles. The coverage and loading of metallic Pt^0 on Co nanowires could be tuned by varying the concentration of Pt^{2+} precursors. Co nanowires with varying coverages of Pt NPs were found to be active in the catalytic degradation of methyl orange (Supporting Information Figure S-2). As the weight ratio of PS-CoNPs to $Pt(acac)_2$ was decreased from 1:1.5 to 1:0.3, a continuous Pt shell encapsulating the cobalt nanoparticle chain was obtained (see Supporting Information Figure S-2), in contrast to the densely packed Pt NPs formed at higher feed ratios, as shown in Figure 1.

The utilization of ferromagnetic cobalt nanoparticles as colloidal monomers in the redox transmetalation reaction was essential to obtain 1-D heterostructured nanowires, as superparamagnetic nanoparticles are unable to polymerize.[76] In earlier reports on transmetalation and galvanic exchange reactions with CoNPs, only continuous shells of metallic Pt with Co cores[62] or Co_xPt_y[80] were investigated for the electroreduction of O_2[73,81] or the electrooxidation of methanol.[69,82,83] However, the synthesis and characterization of high surface area Pt NPs decorated on 1-D nanomaterials to economize the utilization of the platinum catalyst remained largely unexplored.[68,82,84] We also explored the galvanic deposition of AuNPs onto the exterior of Co_3O_4 nanowires using $Au(I)ClPPh_3$ and $HAu(III)Cl_4$ complexes. However, significant etching of CoNPs was observed, which was attributed to either direct oxidation of Co^0 sites by chloride anions from the Au precursor salts or from in situ generated HCl.

Field emission scanning electron microscopy (FE-SEM) was also employed to investigate morphological changes of the PS-CoNPs before and after the exchange reaction with Pt^{2+}. As shown in Figure 2a, the nonagglomerated PS-CoNPs spanning 389 ± 144 nm in length exhibited a smooth surface morphology before the addition of the $Pt(acac)_2$ precursors. After the galvanic reaction with Pt^{2+} at 175 °C for 10 h, FE-SEM revealed a rough surface morphology due to the formation and decoration of Pt NPs around the exterior of the cobalt nanoparticle chains (Figure 2b). Furthermore, FE-SEM imaging (inset Figure 2b) clearly showed features of individual Pt NPs densely packed along the exterior cobalt nanoparticle chains, adopting a raspberry-like roughened morphology, which is consistent with other high surface area nanostructures prepared via galvanic exchange reactions.[82,85,86] In contrast, the magnified FE-SEM images (inset Figure 2a) of the PS-CoNPs exhibited a smooth surface morphology, due to the presence of glassy PS shells and the absence of corrugated surface inclusions on nanoparticle chains.

Heterostructured Platinum−Cobalt Oxide Nanowires. Oxidation reactions were conducted to convert PtNP decorated CoNP chains into hollow cobalt oxide nanowires with Pt inclusions. Initial oxidation reactions were conducted in hot DCB solutions (T = 175 °C), which afforded mixed, amorphous phases of cobalt oxide (Co_xO_y). Using similar conditions to those in our previous reports, a simple oxidation reaction at elevated temperature converted the PtNP coated PS-CoNP chains into heterostructured nanowires composed of PS capping ligands and hollow nanowires containing amorphous cobalt oxide and PtNP (PS-$PtCo_xO_y$ nanowires).[60] After 24 h of solution oxidation at 175 °C, partially hollow nanowires exhibiting a dimensional expansion of 5 nm were formed. The partially hollow PS-$PtCo_xO_y$ nanowires formed via oxidation in solution were imaged via TEM to possess three distinct features: (1) a lower electron density cobalt oxide with a corrugated shell due to Pt NP inclusions, (2) residual unreacted CoNP cores that appeared as dark pear shaped features, and (3) interior voids corresponding to the coalescence of vacancies at the interface (Figure 3a). As the solution-phase oxidation reaction proceeded,

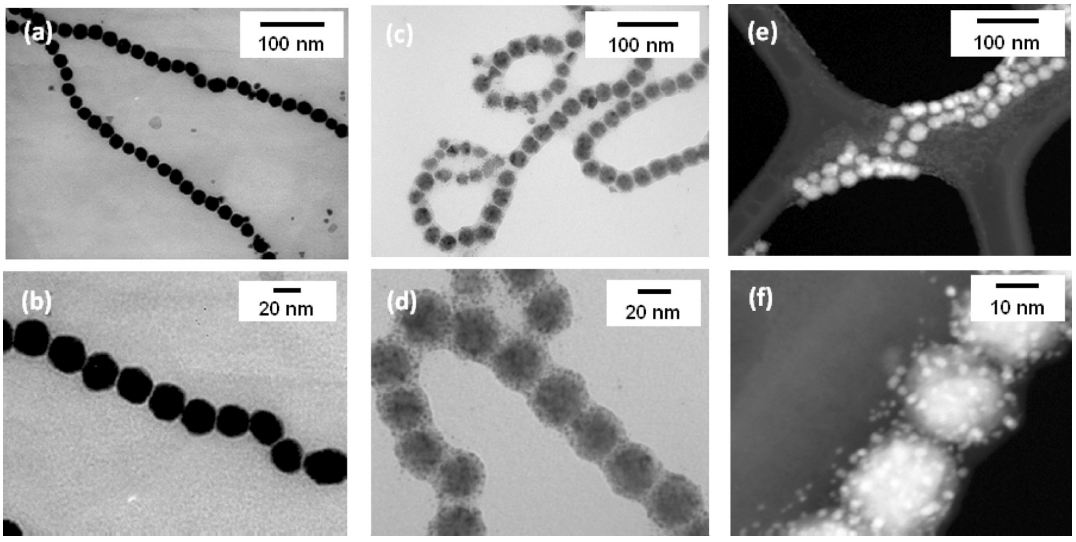

Figure 1. Low and high magnification TEM images of the precursor PS-CoNPs with particle diameter 30 ± 3 nm (a, b); PS-PtCo after the transmetalation reaction, with particle diameter 35 ± 3 nm (c, d); and HAADF-STEM images of the same PS-PtCo, in which the PtNCs appear as bright dots (e, f).

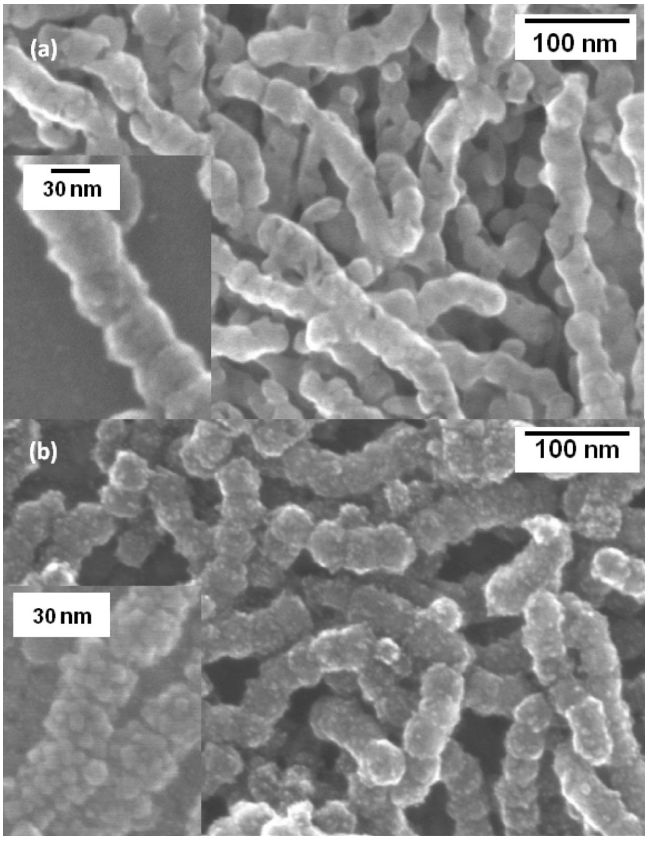

Figure 2. FE-SEM images of (a) PS-CoNPs chains and (b) PS-CoNP chains decorated with Pt NPs after galvanic exchange. Insets in (a) and (b) are high magnification FESEM images of PS-CoNP chain and PS-PtCo chain, respectively.

the oxide shell grew due to the continual diffusion and oxidation of Co at the outermost layer, while leaving a hollow inclusion at the core. This phenomenon was described as the nanoscale Kirkendall effect, which has been widely applied toward the fabrication of various hollow nanostructures.[64,65]

Moreover, the Pt nanocrystallites that were deposited on the outer surfaces of the Co nanoparticle chains (via the first galvanic replacement reaction) were trapped within the cobalt oxide nanowire phase after the oxidation reaction. HR-TEM (Figure 3c,d) and HAADF-TEM (Figure 3e,f) confirmed the encapsulation of Pt NPs within the oxide shell of the 1-D hollow heterostructures. High temperature annealing of PS coated nanowires (T > 300 °C in air) afforded polycrystalline platinum−cobalt oxide nanowires, as observed by TEM, XRD, and XPS as will be discussed in greater detail in later sections. These calcination reactions were limited to temperatures below T = 400 °C, as higher temperatures were observed to result in densification and sintering of the cobalt oxide phase, as observed in our earlier work with core−shell Au−Co_3O_4 nanowires.[59]

Solid-State Characterization of Heterostructured Nanowires. X-ray diffraction (XRD) confirmed the chemical transformation of metallic CoNPs after galvanic and oxidative reactions into bimetallic Pt NP coated CoNP chains and platinum−cobalt oxide nanowires (Figure 4). The XRD of the as-prepared PS-CoNPs precursor showed one broad peak that was assigned to the amorphous fcc-Co phase (Figure 4a). After the treatment with $Pt(acac)_2$ via galvanic exchange, the amorphous fcc-Co phase from CoNPs was observed along with the presence of additional peaks at ∼14° and 26° values of 2θ, which were assigned to fct-CoPt[87] and delta-Co phases, respectively (Figure 4b). Upon solution oxidation of the Pt NP coated CoNP chains at 175 °C in DCB, broad peaks centered at 40° and 24° indicated the formation of a mixture of amorphous fcc-Co, fcc-CoO, fcc-Pt, and fct-PtCo phases. TEM imaging corroborated these XRD findings, as previously discussed (Figure 3), where both residual metallic Co and Co_xO_y were observed in the Pt NP coated CoNP chains after the partial oxidation at 175 °C in DCB. Subsequent calcination of the Pt-Co_xO_y nanowires at 400 °C in air resulted in the formation of polycrystalline platinum−cobalt oxide nanowires, which comprised of Co_3O_4, metallic Pt, and PtO_2 phases (Figure 4d). All diffraction lines assigned in Figure 4d were consistent with standard diffraction peaks reported for the face centered-cubic (fcc) Co_3O_4, Pt, and PtO_2 phases.

dx.doi.org/10.1021/cm102319d |*Chem. Mater.* 2011, 23, 1120–1129

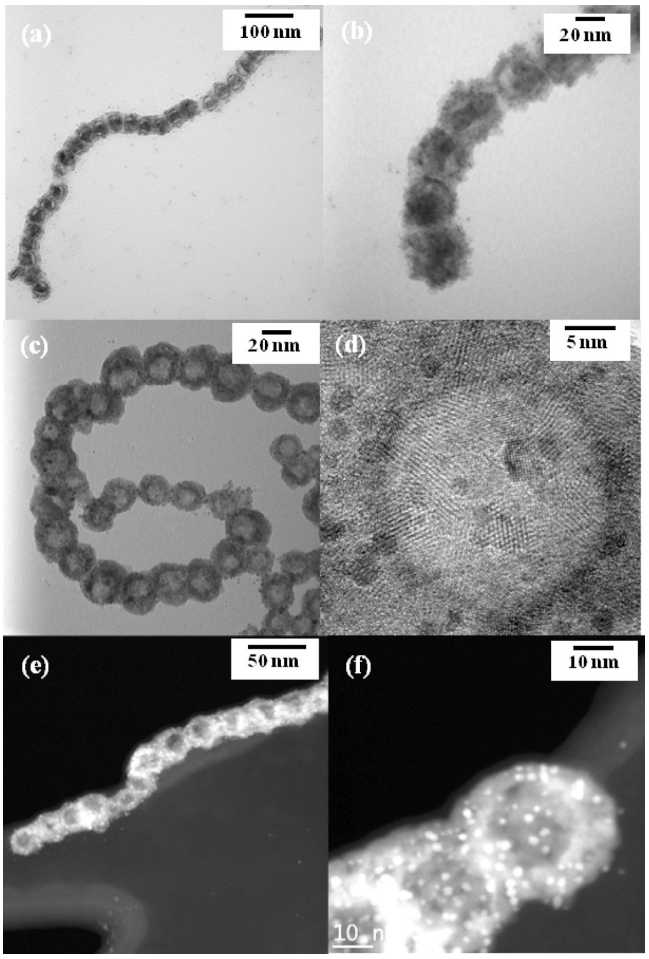

Figure 3. (a) Bright field TEM images of PS capped, Pt-Co_xO_y nanowires ($D = 40 \pm 5$ nm) after solution oxidation at 175 °C in DCB for 24 h, (b) higher resolution bright field TEM of samples from Figure 3a, (c) TEM image of the Pt-Co_3O_4 nanowires after solid state calcination on a carbon coated Cu grid at 300 °C for 30 min, (d) high resolution TEM image of the calcined Pt-Co_3O_4 nanowires in Figure 3c, (e) bright field HAADF-STEM images of the calcined Pt-Co_3O_4 nanowires, (f) high resolution HAADF-STEM image of Figure 3e.

The magnetic properties of these novel 1-D nanomaterials were measured via vibrating sample magnetometry (VSM) at 300 and 50 K. PS-CoNPs precursor materials exhibited weak ferromagnetism at 300 K with a saturation magnetization (M_s) and coercivity (H_c) of 53 emu/g and 831 Oe, respectively (Figure 5a−i). Following the galvanic exchange reaction, the PS capped, PtNP-CoNP chains exhibited a similar hysteresis curve with a slight decrease in magnetization and coercivity (M_s = 51 emu/g and H_c = 353 Oe) due to the replacement of the magnetic Co core with the PtNPs (Figure 5a-ii). In the conversion of the magnetic PtCo to Pt-Co_3O_4 metal−semiconductor materials, the magnetic properties significantly decreased, which was in agreement with the formation of paramagnetic cobalt oxides at room temperature. After 24 h of oxidation at 175 °C in DCB, PS capped PtCo_xO_y nanowires were observed to exhibit a significantly diminished magnetization (M_s = 14 emu/g at 300 K) but were also weakly ferromagnetic (H_c = 330 Oe at 300 K) (Figure 5a-iii) at room temperature. This ferromagnetic behavior was attributed to the presence of trace metallic Co (refer to TEM images in Figure 2a,b).[88] Upon calcination at

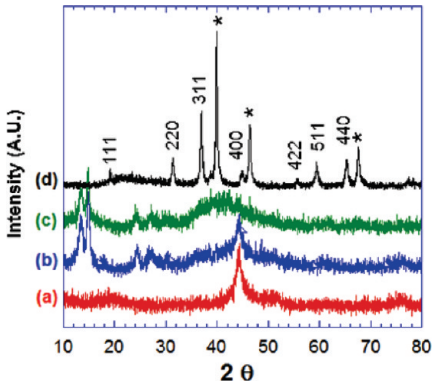

Figure 4. Overlay of XRD patterns of (a) PS-CoNPs nanoparticles with fcc-Co, (b) PS-PtCo nanowires after the galvanic exchange reaction, (c) PS-PtCoO nanowires after solution oxidation at 175 °C for 24 h, (d) Pt-Co_3O_4 nanowires after calcination at 400 °C for 12 h in static air showing the polycrystalline phase of Co_3O_4, PtO_2 and metallic Pt. The diffraction peaks in (d) were indexed to the fcc-Co_3O_4 phase (black indexes) while red indexes referred to metallic Pt and PtO_2 diffractions.

400 °C for 12 h, the saturation magnetization further decreased to 0.466 emu/g while retaining a hysteresis curve with H_c = 267 Oe (Figure 5a-iv,b). The observation of weakly ferromagnetic behavior from calcined Pt-Co_3O_4 nanowires at 300 K was surprising in comparison to the paramagnetic behavior exhibited by hollow Co_3O_4 nanowires.[60] Since both of these materials (i.e., Pt and Co_3O_4) are not ferromagnetic, we attributed this magnetic behavior to the presence of trace bimetallic phases of CoPt, which may exhibit different oxidative and magnetic properties than CoNP based systems.

Spectroscopic Characterization of Pt-Co_3O_4 Nanowires. X-ray photoelectron spectroscopy (XPS) was conducted to analyze the valence states of elements on the surfaces of these metal−semiconductor oxide heterostructures to correlate their surface compositions with electrochemical characterization. It has been well established that the growth of surface oxides on Pt metal changes their electronic properties by imposing a barrier to charge transfer and influencing the adsorption of reactants at the catalytic surfaces through site blocking effects.[89,90] As bulk XRD measurements indicated that calcination of Pt-Co_xO_y nanowires at T = 400 °C in air for 12 h afforded nanocomposites with both metallic Pt and PtO_2 phases, we conducted a series of kinetic experiments using XPS to determine optimal reaction times to maximize the formation of Co_3O_4, while minimizing the formation of PtO_2. All of these XPS measurements were conducted on nanowire thin films deposited onto Si wafers and measured in the Co 2p and Pt 4f binding energy regions after various calcination conditions. Initially, processing conditions used for Co_3O_4 nanowires from our previous report[60] were conducted, where films of PS capped PtNP-CoNP chain films calcined at 400 °C for 12 h and were immediately analyzed via XPS. In the Co 2p binding energy region, two major $2p_{3/2}$ and $2p_{1/2}$ spin−orbit peaks appeared at 796.1 and 780.6 eV, respectively, accompanied by weaker satellite peaks at 790.5 and 805.5 eV, which were consistent with our previous report (Figure 6e).[60] However, under these calcination conditions, the Pt 4f binding energy region showed three overlapping peaks, which were assigned to metallic Pt, PtO, and PtO_2 with respective Pt $4f_{7/2}$ binding energies at 72, 75, and 78 eV (with relative compositions of 47%, 17%, and 37%, Figure 6e).[87] On the basis of these assignments and their respective relative intensities, a high

dx.doi.org/10.1021/cm102319d |*Chem. Mater.* 2011, 23, 1120–1129

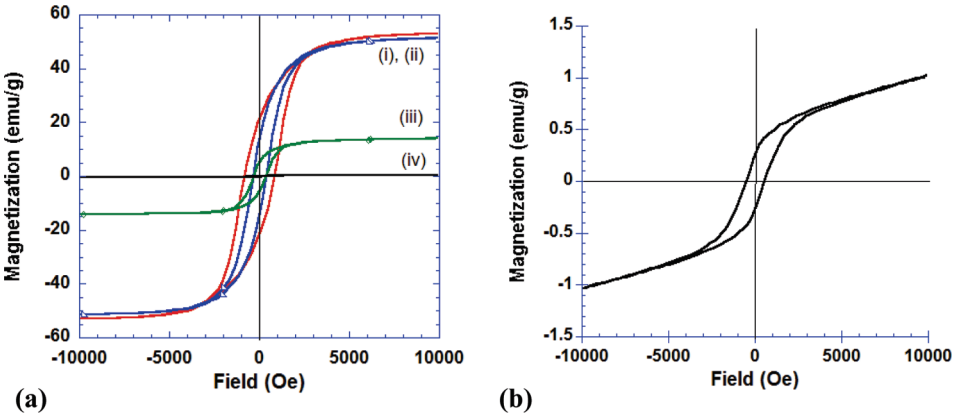

Figure 5. Overlay of hysteresis curves of applied field (H) versus magnetization (M_s) of the metal/semiconductor oxide heterostructures at 300 K. (a-i) PS-CoNPs, (a-ii) PS-PtCo nanowires, (a-iii) PS-PtCoO nanowires oxidized at 175 °C, (a-iv) PtO-Co_3O_4 nanowires calcined at 400 °C for 12 h. Part (b) shows the magnified hysteresis curve of the calcined PtO-Co_3O_4 at 300 K.

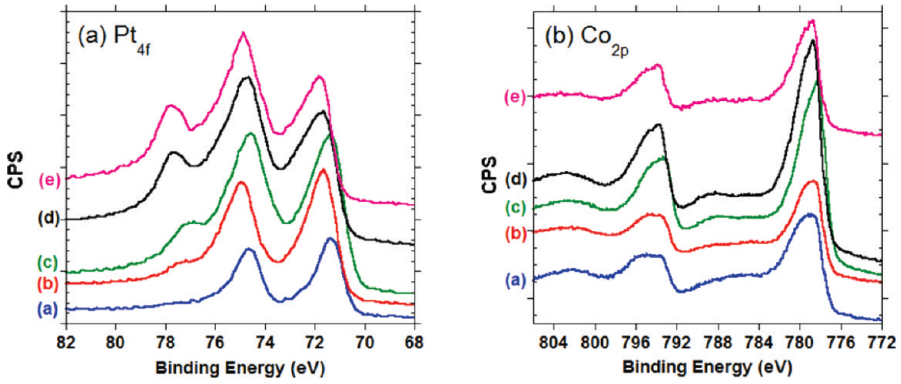

Figure 6. XPS spectra in the Pt 4f and Co 2p regions of the PtCo and Pt-Co_3O_4 under varying calcination conditions: PS-PtCo films (a) calcined under argon, (b) calcined in air at 300 °C for 15 min, (c) calcined in air at 300 °C for 30 min, (d) calcined in air at 400 °C for 60 min, and (e) calcined in air at 400 °C for 12 h.

fraction of Pt oxide phases was observed to be formed when PS capped Pt-Co_xO_y nanowires were calcined T = 400 °C in air for 12 h.

To suppress the formation of Pt oxide phases, calcinations of PS capped, Pt-Co_xO_y nanowires at varying temperatures (T = 300, 400 °C in air) and reaction times were conducted and monitored using XPS (Figure 6). Optimal processing conditions to form Pt-Co_3O_4 nanowires were determined to form at T = 300 °C for 30 min, although both PtO and PtO_2 phases were still formed, as noted by XPS of Pt4$f_{7/2}$ binding energies at 77 and 78 eV (Figure 6c). Calcination experiments conducted at T = 400 °C indicated that significant formation of PtO and PtO_2 phases was observed for reaction times longer than 60 min, as noted from XPS (Figure 6d,e). XPS analysis was also conducted on thin films of PtNP decorated PS-CoNP chains calcined in argon at 400 °C for 12 h in the Co 2p and Pt 4f binding energy regions which revealed two peaks with binding energies at 73 and 76.3 eV in the Pt 4f region, which corresponded to the electronic states of 4$f_{7/2}$ and 4$f_{5/2}$ in metallic Pt, respectively (Figure 6a). Additionally, the energy difference between the two peaks is about 3.3 eV,[91] which also confirmed that the majority of the Pt existed in the metallic Pt^0 phase when the calcination was performed under argon. Table S-1 (see Supporting Information) summarizes the relative intensities of the metallic Pt and platinum oxides based on the Pt 4$f_{7/2}$ binding energies (Figure 6) for PtCo heterostructures calcined under varying conditions. The formation of the Co_3O_4 phase under the optimized calcination conditions was confirmed via XPS analysis (Figure 6c, which has been extensively observed in thin films of cobalt oxides[92−95]) and cyclic voltammetry characterization (Figure 7), which will be discussed in the following section.

Cyclic Voltammetry of the Calcined Pt-Co_3O_4 Nanowire Films on ITO. The electrochemical properties of the calcined Pt-Co_3O_4 metal−semiconductor heterostuctures and the hollow Co_3O_4 nanowires were characterized via cyclic voltammetry (CV). The modified films were deposited onto ITO, calcined, and cycled at 20 mV/s from 0.6 V to −0.9 V with respect to an Ag/AgCl (3 M KCl) reference electrode in 1 M NaOH electrolyte solution. On the basis of our previous calcination studies, the most optimal calcination condition (300 °C in air for 30 min) was employed for both Pt-Co_3O_4 and Co_3O_4 nanowires prior to the cyclic voltammetry experiments. Figure 7 shows the overlaid cyclic voltammograms of the Pt-Co_3O_4 (red curve) and Co_3O_4 (blue curve) nanowires in alkaline solution, which were normalized based on the number of nanoparticles per electrode area (Supporting Information, Figure S-4, for representative FESEM images used to analyze chain lengths and number of nanoparticles). Under the optimal calcination conditions, both voltammograms exhibited multiple redox peaks corresponding to different oxidation states of

dx.doi.org/10.1021/cm102319d |*Chem. Mater.* 2011, 23, 1120–1129

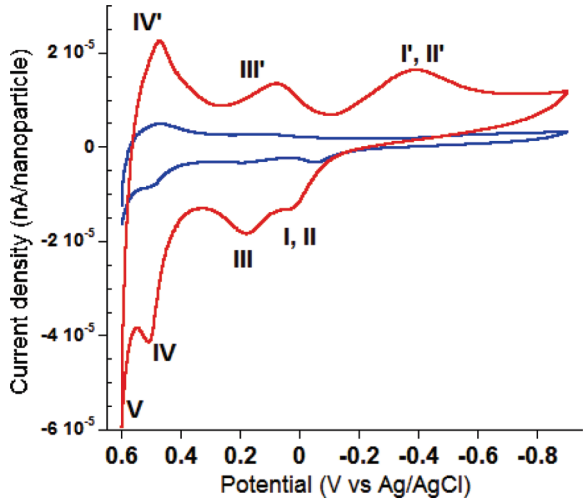

Figure 7. (a) Overlay of cyclic voltammograms from Co_3O_4 (blue trace) and the Pt-Co_3O_4 (red trace) thin films on ITO calcined at 300 °C for 30 min. Redox phases of cobalt oxides and platinum are assigned with Roman numerals I−V corresponding to the electrochemical reactions illustrated in eqs 1−9. The voltammetric curves were normalized based on the surface coverage of nanoparticles per electrode area.

cobalt oxides in alkaline media. The voltammogram of the Co_3O_4 (blue curve) shows three sets of cathodic and anodic peaks, which corresponded to the signature redox peaks of $Co(OH)_2$, Co_3O_4, CoOOH, and CoO_2 at −0.32, 0, 0.17, and 0.5 V, respectively. The assignments of these peaks were consistent with previously reported redox behavior of cobalt oxides in alkaline media and can be associated with the following reactions.[53,60,96−98]

Anodic scan (toward positive potentials)

Peak I (0 V) → Co_3O_4 formation:

$$3Co(OH)_2 + 2OH^- \rightleftharpoons Co_3O_4 + 4H_2O + 2e^- \quad (1)$$

Peak II $(0-0.17V) \rightarrow Pt(OH)$ *adsorption and* PtO_x *formation*

$$Pt + OH^- \rightleftharpoons Pt - OH_{ads} + H_2O + e^-$$

$$Pt - OH_{ads} \rightleftharpoons PtO_x + H_2O + e^- \quad (2)$$

Peak III (0.17 V) → CoOOH formation:

$$Co_3O_4 + OH^- + H_2O \rightleftharpoons 3CoOOH + e^- \quad (3)$$

Peak IV (0.5 V) → CoO_2 formation:

$$3CoOOH + OH^- \rightleftharpoons CoO_2 + H_2O + e^- \quad (4)$$

Peak V (0.6 V) → oxygen evolution:

$$4^- OH \rightleftharpoons O_2 + 2H_2O + 4e^- \quad (5)$$

Cathodic scan (toward negative potentials)

Peak IV′ (0.47 V) → CoOOH formation:

$$CoO_2 + H_2O + e^- \rightleftharpoons CoOOH + OH^- \quad (6)$$

Peak III′ (0.07 V) → Co_3O_4 formation:

$$3CoOOH + e^- \rightleftharpoons Co_3O_4 + OH^- + H_2O \quad (7)$$

Peak II′ (−0.32 V) → $Co(OH)_2$ formation:

$$Co_3O_4 + H_2O + 2e^- \rightleftharpoons 3(Co(OH)_2 + 2OH^- \quad (8)$$

Peak I′ (−0.4 V) → reduction PtO_x

$$PtO_x + H_2O + 2e^- \rightleftharpoons PtO_{(x-1)} + 2OH^- \quad (9)$$

Specifically, the cyclic voltammogram of the hybrid Pt-Co_3O_4 nanowires film (red curve) obtained in 1 M NaOH was also dominated by the redox peaks from the cobalt oxides accompanied with a sharp oxygen evolution reaction at ≈0.6 V (peak V). On the basis of electrochemical investigations of Pt in alkaline media, the broad cathodic peak at around −0.4 V could be assigned to the reduction of the Pt^{2+} oxide layer to Pt^0 (peak I′), which is insignificant in the CV of the pristine Co_3O_4 nanowires (blue trace).[82,99,100] In the reverse potential sweep, the formation of platinum oxides or the adsorption of hydroxide (OH^-) species (peak I) overlapped with the oxidation of $Co^{2+/3+}$ and Co^{3+} at 0 and 0.17 V, respectively.[82,89,101,102] Following the adsorption of the OH^- species, the irreversible Pt oxide formation was speculated to be overlapping with the oxidation of $Co^{3+} \rightarrow Co^{4+}$ and the oxygen evolution reaction (OER) in the potential region of 0.2−0.6 V. The lack of hydrogen adsorption and desorption features arising from the PtNCs has also been suggested to be affected by the presence of contaminants,[99] crystallinity, and particle size of the PtNCs.[11,99,102,103] Similarly, Nam and Belcher et al. primarily observed the electrochemical activity of Co_3O_4 phases in the CV of the AuNP coated Co_3O_4 nanowires that were prepared via the virus templating method.[44] The observation of enhanced Co_3O_4 redox processes in the CV of Pt-Co_3O_4 nanowires could also be attributed to the inherent composition and the porosity of the nanowires that contributed to the formation of high electroactive surface area thin films on ITO. Nevertheless, the incorporation of the noble metal into the Co_3O_4 played a significant role in enhancing the electronic conductivity of Co_3O_4 nanowires via several possible mechanisms: (1) higher conductivity of Pt NPs which enhanced electron transport, (2) the presence of Pt which increased the number of dislocation and imperfections in the crystal structure of Co_3O_4, allowing for electronic transitions to proceed more readily, thus increasing electrical conductivity,[57] and (3) lowering of the contact resistance between the nanowires and ITO, resulting in the enhancement of current density in the cyclic voltammetry relative to the pristine Co_3O_4 nanowires.[104−106] Although the exact contribution of PtNPs has yet to be determined, our results suggested that the homogeneous dispersion of PtNCs within the Co_3O_4 nanowires exhibited a sevenfold enhancement in specific capacitance over the hollow Co_3O_4 nanowires (see Supporting Information for particle count and calculation; Table S-2 for a summary of specific capacitances determined from cyclic voltammetry). However, under calcination at 400 °C for 12 h in air, the CV of the 1-D PtO-Co_3O_4 exhibited only two redox couples corresponding to the electrochemical reactions of platinum oxides (eq 2) and CoO_2 (eq 4) (Supporting Information, Figure S-3). The formation of platinum oxides under this calcination condition was also supported by both XRD and XPS (Figures 4 and 6, respectively). The differences in electrochemical behavior emphasized the detrimental effect of prolonged calcinations in air at

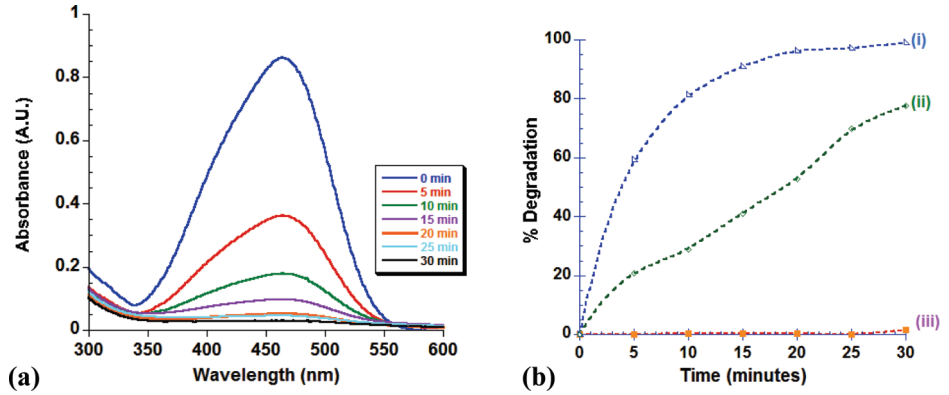

Figure 8. (a) Evolution of the UV−vis absorption spectrum of 26 μM methyl orange (λ_{max} = 466 nm) in the presence of 0.4 mg of $PtCo_3O_4$ calcined in air at 300 °C for 30 min. Each absorbance was taken at a predetermined reaction time over a period of 30 min. (b) Kinetics plot of the hydrogenation of 26 μM methyl orange over PS-PtCo (0.4 mg) calcined at different conditions: (i) Pt-Co_3O_4, calcined in air at 300 °C for 30 min, (ii) PtO-Co_3O_4, calcined in air at 400 °C for 12 h, and (iii) Co_3O_4, calcined in air at 400 °C for 12 h. The kinetic data points were fitted with a smooth curve function.

elevated temperatures on the structures and properties of these 1-D heterostructures. This result was attributed to the formation of platinum oxides, which dampened the electrical properties of the heterostructured nanowires, as well as the electrochemical activities of the Co_3O_4 phases, which explained the lack of redox features arising from the Co_3O_4 phases in Figure S-3 (Supporting Information).[87] The reduced electrochemical activity of PtO-Co_3O_4 at higher calcination temperatures was also attributed to the collapse of the porosity in the nanowires shell, which reduced the number of electroactive sites. Furthermore, the specific capacitance of the Pt-Co_3O_4 was found to decrease from 12.5×10^{-5} farads to 7.6×10^{-5} farads (per nanoparticle) in the anodic scan, upon increasing the calcination temperature and time from 300 °C for 30 min to 400 °C for 12 h, respectively. Similar trends were also observed in the catalytic activities of these 1-D heterostructures, in which the hydrogenation rate decreased with excessive formation of Pt oxides upon prolonged oxidations (discussed in the following section).

Catalytic Hydrogenation of Methyl Orange. To confirm the accessibility and reactivity of PtNPs embedded within the cobalt oxide nanowires, hydrogenation of methyl orange was investigated at room temperature. Methyl orange, a water-soluble dye, served as a model compound to evaluate the catalytic activity of calcined nanowires at various conditions, as the cleavage of the diazo bonds resulted in a colorimetric change of solutions from orange to colorless. The porous nature of the cobalt oxide shell allowed for the hydrogen saturated methyl orange solutions to permeate through the shell and react with the PtNPs. In this study, the hydrogenation rate was followed by monitoring the change in the absorbance of methyl orange (λ_{max} = 466 nm) via UV−vis absorption spectroscopy (Figure 8a). The concentration of methyl orange was determined by generating a UV−vis calibration curve (R^2 = 0.999) with known concentration of methyl orange solutions. The comparative kinetics of the degradation of methyl orange in the presence of nanowire catalysts processed using different calcination conditions (400 °C in argon for 12 h, 300 °C in air for 30 min, 400 °C in air for 12 h) were investigated. Control experiments with calcined hollow Co_3O_4 nanowires were also conducted (Figure 8b). Heterostructured nanowire catalysts that were calcined in air at T = 300 °C for 30 min were observed to degrade methyl orange to a conversion of 80% after 10 min (Figure 8b-i), while nanowire catalysts calcined in air at T = 400 °C for 12 h exhibited significantly reduced activity as noted by modest conversions of 20% after 10 min (Figure 8b-ii). Control experiments with only hollow Co_3O_4 nanowires as catalysts showed negligible degradation of methyl orange solution under the same conditions (Figure 8b-iii), which confirmed that the hydrogenation reactions were only catalyzed by accessible PtNPs that were embedded within the cobalt oxide shells (see TEM and STEM in Figure 3). Additionally, these experiments also confirmed that the cobalt oxide shells were indeed porous, allowing for the diffusion of the hydrogen saturated methyl orange in and out of the oxide shell. As reported by Alivisatos and co-workers, the reactants most likely permeated through the grain boundaries of the cobalt oxide shell and catalytically hydrogenated at the surfaces of PtNPs that were trapped within the interior of the oxide shell.[65] The trend showed that the catalytic performance was also dependent on the calcination conditions, as enriched compositions of metallic Pt resulted in the higher catalytic activity.

CONCLUSIONS

In summary, we have demonstrated the colloidal polymerization of ferromagnetic nanoparticles into metal−semiconductor nanowires comprised of platinum nanocrystallites confined within the hollow cobalt oxide nanowires. By combining dipolar assembly, a galvanic replacement reaction, and a nanoscale Kirkendall oxidation reaction, heterostructured nanowires were synthesized. The 1-D Pt-Co_3O_4 heterostructured electrodes exhibited sevenfold enhancement in the specific capacitance in comparison to the pristine Co_3O_4 nanowires. We also demonstrated that the electrochemical and catalytic activities of the Pt-Co_3O_4 nanowires were dependent on the surface composition of the Pt inclusions, as dictated by processing conditions to prepare these materials. The colloidal polymerization methodology reported in this work provides a facile approach toward the synthesis of hybrid nanowires with controlled composition and morphology, thus allowing for structure−property interrogation of the metal−semiconductor interfaces.

ASSOCIATED CONTENT

Supporting Information. UV−vis absorbance, TEM and HAADF-STEM images, XPS, and cyclic voltammetry (PDF). This material is available free of charge via the Internet at http://pubs.acs.org.

dx.doi.org/10.1021/cm102319d |*Chem. Mater.* 2011, 23, 1120–1129

■ ACKNOWLEDGMENT

The NSF CAREER Program (DMR-0645618), the ONR-YIP (N00014-07-1-0796), the World Class University program through the National Research Foundation of Korea funded by the Ministry of Education, Science and Technology (R31-10013), DOE-BES (DE-FG03-02ER15753), and the Alfred P. Sloan Foundation are acknowledged for synthetic support of this work.

■ REFERENCES

(1) Cozzoli, P. D.; Pellegrino, T.; Manna, L. *Chem. Soc. Rev.* **2006**, *35*, 1195–1208.
(2) Casavola, M.; Buonsanti, R.; Caputo, G.; Cozzoli, D. *Eur. J. Inorg. Chem.* **2008**, 837–854.
(3) Bard, A. J. *J. Phys. Chem.* **1982**, *86* (2), 172–177.
(4) Bard, A. J. *J. Electroanal. Chem.* **1984**, *168*, 5–20.
(5) Nozik, A. J. *Appl. Phys. Lett.* **1977**, *30*, 567–569.
(6) Heller, A.; Aharon-Shalom, E.; Bonner, W. A.; Miller, B. *J. Am. Chem. Soc.* **1982**, *104* (25), 6942–6948.
(7) Kamat, P. *J. Phys. Chem. C* **2007**, *111*, 2834–2860.
(8) Kamat, P. *J. Phys. Chem. C* **2008**, *112*, 18737–18753.
(9) Mokari, T.; Rothenberg, E.; Popov, I.; Costi, R.; Banin, U. *Science* **2004**, *304*, 1787–1790.
(10) Mokari, T.; Sztrum, C. G.; Salant, A.; Rabani, E.; Banin, U. *Nat. Mater.* **2005**, *4*, 855–863.
(11) Mills, A.; Lee, S. K. *Platinum Met. Rev.* **2003**, *47*, 2–12.
(12) Kortan, A. R.; Hull, R.; Opila, R. L.; Bawendi, M. G.; Steigerwald, M. L.; Carroll, P. J.; Brus, L. E. *J. Am. Chem. Soc.* **1990**, *112*, 1327–1332.
(13) Peng, X. G.; Schlamp, M. C.; Kadavanich, A. V.; Alivisatos, A. P. *J. Am. Chem. Soc.* **1996**, *119*, 7019.
(14) Subramanian, V.; Wolf, E. E.; Kamat, P. *J. Phys. Chem. B* **2003**, *107* (30), 7479–7485.
(15) Subramanian, V.; Wolf, E. E.; Kamat, P. *Langmuir* **2003**, *19*, 469–474.
(16) Wood, A.; Giersig, M.; Mulvaney, P. *J. Phys. Chem. B* **2001**, *105*, 8810–8815.
(17) Dawson, A.; Kamat, P. *J. Phys. Chem. B* **2001**, *105*, 960–966.
(18) Teranishi, T.; Inoue, Y.; Nakaya, M.; Oumi, Y.; Sano, T. *J. Am. Chem. Soc.* **2006**, *126*, 9914–9915.
(19) Choi, S.-H.; Kim, E.-G.; Hyeon, T. *J. Am. Chem. Soc.* **2006**, *126*, 2520–2521.
(20) Kwon, K.-W.; Shim, M. *J. Am. Chem. Soc.* **2005**, *127*, 10269–10275.
(21) Pellegrino, T.; Fiore, A.; Carlino, E.; Giannini, C.; Cozzoli, D.; Ciccarella, G.; Respaud, M.; Palmirotta, L.; Cingolani, R.; Manna, L. *J. Am. Chem. Soc.* **2006**, *128*, 6690–6698.
(22) Wang, C.; Xu, C.; Zeng, H.; Sun, S. *Adv. Mater.* **2009**, *21*, 1–8.
(23) Gu, H.; Zheng, R.; Zhang, X.; Xu, B. *J. Am. Chem. Soc.* **2004**, *126*, 5664–5665.
(24) Yu, H.; Chen, M.; Rice, P. M.; Wang, S. X.; White, R. L.; Sun, S.-H. *Nano Lett.* **2005**, *5*, 379–382.
(25) Choi, S.-H.; Na, H. B.; Park, Y. I.; An, K.; Kwon, S. G.; Jang, Y.; M.-H., P.; Moon, J.; Son, J. S.; C., S. I.; Moon, W. K.; Hyeon, T. *J. Am. Chem. Soc.* **2008**, *130*, 15573–15580.
(26) Shi, W.; Zeng, H.; Sahoo, Y.; Ohulchanskyy, T. Y.; Ding, Y.; Wang, Z. L.; Swihart, M.; Prasad, P. N. *Nano Lett.* **2006**, *6*, 875–881.
(27) Costi, R.; Saunders, A. E.; Banin, U. *Angew. Chem., Int. Ed.* **2010**, *49* (29), 4878–4897.
(28) Buonsanti, R.; Grillo, V.; Carlino, E.; Giannini, C.; Curri, M. L.; Innocenti, C.; Sangregorio, C.; Achterhold, K.; Parak, F. G.; Agostiano, A.; Cozzoli, D. *J. Am. Chem. Soc.* **2006**, *128*, 16953–16970.
(29) Kudera, S.; Carbone, L.; Casula, M. F.; Cingolani, R.; Falqui, A.; Snoeck, E.; Parak, W. J.; Manna, L. *Nano Lett.* **2005**, *5*, 445–449.
(30) Casavola, M.; Grillo, V.; Carlino, E.; Giannini, C.; F., G.; Pinel, E. F.; Garcia, M. A.; Manna, L.; Cingolani, R.; Cozzoli, D. *Nano Lett.* **2007**, *7*, 1386–1395.
(31) Habas, S. E.; Yang, P. D.; Mokari, T. *J. Am. Chem. Soc.* **2008**, *130*, 3294–3295.
(32) Deka, S.; Falqui, A.; Bertoni, G.; Sangregorio, C.; Poneti, G.; Morello, G.; Giorgi, M. D.; Giannini, C.; Cingolani, R.; Manna, L.; Cozzoli, D. *J. Am. Chem. Soc.* **2009**, *131*, 12817–12828.
(33) Elmalem, E.; Saunders, A. E.; R., C.; Salant, A.; Banin, U. *Adv. Mater.* **2008**, *20*, 1–6.
(34) Plante, I. J.-L.; Habas, S. E.; Yuhas, B. D.; Gargas, D. J.; Mokari, T. *Chem. Mater.* **2009**, *21*, 3662–3667.
(35) Talapin, D. V.; Shevchenko, E. V.; Lobo, A.; Murray, C. B. *J. Phys. Chem. C* **2007**, *111*, 14049–14055.
(36) Costi, R.; Saunders, A. E.; Elmalem, E.; Salant, A.; Banin, U. *Nano Lett.* **2008**, *8*, 637–641.
(37) Amirav, L.; Alivisatos, A. P. *J. Phys. Chem. Lett.* **2010**, *111*, 1051–1054.
(38) Steiner, D.; Mokari, T.; Banin, U.; Millo, O. *Phys. Rev. Lett.* **2005**, *95*, 056805.
(39) Yin, Y.; Alivisatos, A. P. *Nature* **2005**, *437*, 664–670.
(40) Guo, Y.-G.; Hu, J.-S.; Wan, L.-J. *Adv. Mater.* **2008**, *20*, 2878–2887.
(41) Osterloh, F. E. *Chem. Mater.* **2008**, *20*, 35–54.
(42) Bruce, P. G.; Scrosati, B.; Tarascon, J.-M. *Angew. Chem., Int. Ed.* **2008**, *47*, 2930–2946.
(43) Long, J. W.; Dunn, B.; Rolison, D. R.; White, H. S. *Chem. Rev.* **2004**, *104*, 4463–4492.
(44) Nam, K. T.; Kim, D.-W.; Yoo, P. J.; Chiang, C.-Y.; Meethong, N.; Hammond, P. T.; Chiang, Y.-M.; Belcher, A. M. *Science* **2006**, *312* (5775), 885–888.
(45) Zheng, M.-B.; Cao, J.; Liao, S.-T.; Liu, J.-S.; Chen, H.-Q.; Zhao, Y.; Dai, W.-J.; Ji, G.-B.; Cao, J.-M.; Tao, J. *J. Phys. Chem. C* **2009**, *113*, 3887–3894.
(46) Kandalkar, S. G.; FGunjakar, J. L.; Lokhande, C. D. *Appl. Surf. Sci.* **2008**, *254*, 5540–5544.
(47) Alexander, B. D.; Kulesza, P. J.; Solarskac, R.; Augustynski, J. *J. Mater. Chem.* **2008**, *18*, 2298–2303.
(48) Kanan, M. W.; Nocera, D. G. *Science* **2008**, *321*, 1072–1075.
(49) Castro, E. B.; Gervasi, C. A.; Vilche, J. R. *J. Appl. Electrochem.* **1998**, *28*, 835–841.
(50) Woodhouse, M.; Herman, G. S.; Parkinson, B. A. *Chem. Mater.* **2005**, *17*, 4318–4324.
(51) Walsh, A.; Ahn, K.-S.; Shet, S.; Huda, M. N.; Deutsch, T. G.; Wang, H.; Turner, J. A.; Wei, S.-H.; Yan, Y.; Al-Jassim, M. M. *Energy Environ. Sci.* **2009**, *2*, 774–782.
(52) Tuysuz, H.; Comotti, M.; Schuth, F. *Chem. Commun.* **2008**, 4022–4024.
(53) Svegl, F.; Orel, B.; Hutchins, M. G.; Kalcher, K. *J. Electrochem. Soc.* **1996**, *143*, 1532–1539.
(54) Estrada, W.; Fantini, M. C. A.; de Castro, S. C.; Polo da Fonseca, C. N.; Gorenstein, A. *J. Appl. Phys.* **1993**, *74*, 5835–5841.
(55) Hardee, K. L.; Bard, A. J. *J. Electrochem. Soc.* **1977**, 215–224.
(56) Hu, J.; Wen, Z.; Wang, Q.; Yao, X.; Zhang, Q.; Zhou, J.; Li, J. *J. Phys. Chem. B* **2006**, *110*, 24305–24310.
(57) Svegl, F.; Orel, B.; Grabec-Svegl, I.; Kaucic, V. *Electrochim. Acta* **2000**, *45*, 4359–4371.
(58) Matsui, T.; Kamiuchi, N.; Fujiwara, K.; Kikuchi, R.; Eguchi, K. *J. Electrochem. Soc.* **2009**, *156*, K128–K133.
(59) Kim, B. Y.; Shim, I.-B.; Araci, Z. O.; Saavedra, S. S.; Monti, L. A.; Armstrong, A.; Sahoo, R.; Srivastava, D. N.; Pyun, J. *J. Am. Chem. Soc.* **2010**, *132*, 3234–3235.
(60) Keng, P. Y.; Kim, B. Y.; Shim, I.-B.; Sahoo, R.; Veneman, P. E.; Armstrong, N. R.; Yoo, H.; Pemberton, J. E.; Bull, M. M.; Griebel, J. J.; Ratcliff, E. L.; Nebesny, K. G.; Pyun, J. *ACS Nano* **2009**, *3*, 3143–3157.
(61) Sun, Y. G.; Mayers, B. T.; Xia, Y. *Adv. Mater.* **2003**, *15*, 641–646.
(62) Park, J.-I.; Cheon, J. *J. Am. Chem. Soc.* **2001**, *123*, 5743–5746.
(63) Smigelskas, A. D.; Kirkendall, E. O. *Trans. AIME* **1947**, *171*, 130.
(64) Fan, H. J.; Gosele, U.; Zacharias, M. *Small* **2007**, *3* (10), 1660–1671.
(65) Yin, Y.; Rioux, R. M.; Erdonmez, C. K.; Hughes, S.; Somorjai, G. A.; Alivisatos, A. P. *Science* **2004**, *304* (5671), 711–714.

(66) Sun, Y.; Mayers, B. T.; Xia, Y. *Nano Lett.* **2002**, *2*, 481–485.
(67) Liang, H.-P.; Guo, Y.-G.; Zhang, H.-M.; Hu, J.-S.; Bai, C.-L. *Chem. Commun.* **2004**, 1496–1497.
(68) Liang, H.-P.; Lawrence, N. S.; Wan, L.-J.; Jiang, L.; Song, W.-G.; Jones, T. G. *J. Phys. Chem. C* **2008**, *112*, 338–344.
(69) Liang, H.-P.; Zhang, H.-M.; Hu, J.-S.; Guo, Y.-G.; Wan, L.-J.; Bai, C.-L. *Angew. Chem., Int. Ed.* **2004**, *43*, 1540–1543.
(70) Skrabalak, S. E.; J., C.; Sun, Y.; Lu, X.; Au, L.; Cobley, C. M.; Xia, Y. *Acc. Chem. Res.* **2008**, *41*, 1587–1595.
(71) Yin, Y.; Erdonmez, C. K.; Aloni, S.; Alivisatos, A. P. *J. Am. Chem. Soc.* **2006**, *128*, 12671–12673.
(72) Vasquez, Y.; Sra, A. K.; Schaak, R. E. *J. Am. Chem. Soc.* **2005**, *127*, 12504–12505.
(73) Zhai, J.; Huang, M.; Zhai, Y.; Dong, S. *J. Mater. Chem.* **2007**, *18*, 923–928.
(74) Zeng, J.; Huang, J.; Lu, W.; Wang, X.; Wang, B.; Zhang, S.; Hou, J. *Adv. Mater.* **2007**, *19*, 2172–2176.
(75) Schwartzberg, A. M.; Olson, T. Y.; Talley, C. E.; Zhang, J. Z. *J. Phys. Chem. C* **2007**, *111* (44), 16080–16082.
(76) Gao, J.; Zhang, B.; Zhang, X.; Xu, B. *Angew. Chem., Int. Ed.* **2006**, *45* (8), 1220–1223.
(77) Yin, Y.; Erdonmez, C. K.; Cabot, A.; Hughes, S. M.; Alivisatos, A. P. *Adv. Funct. Mater.* **2006**, *16*, 1389–1399.
(78) Bull, M. M.; Chung, W.-J.; Rasmussen, S. G.; Kim, S.-J.; Shim, I.; Paik, H. J.; Pyun, J. *J. Mater. Chem.* **2010**, *20*, 6023–6025.
(79) Vanysek, P. *In handbook of chemistry and physics*; CRC Press: Boca Raton, 1995; pp 8−21.
(80) Park, J.-I.; Kim, M. G.; Jun, Y.-W.; Lee, J. S.; Lee, W.-R.; Cheon, J. *J. Am. Chem. Soc.* **2004**, *126*, 9072–9078.
(81) Chen, S.-C.; Ferreira, P. J.; Sheng, W.; Yabuuchi, N.; Allard, L.; Yanf, S.-H. *J. Am. Chem. Soc.* **2008**, *130*, 13818–13819.
(82) Chen, Q.-S.; Sun, S.-G.; Zhou, Z.-Y.; Chen, Y.-S.; Deng, S.-B. *Phys. Chem. Chem. Phys.* **2008**, *10*, 3645–3654.
(83) Liu, L.-F.; Pippel, E.; Scholz, R.; Gosele, U. *Nano Lett.* **2009**, *9*, 4352–4358.
(84) Guo, S.; Dong, S.; Wang, E. *Chem.—Eur. J.* **2008**, *14*, 4689–4695.
(85) Chen, J.; Wiley, B.; McLellan, J.; Xiong, Y.; Li, Z.-Y.; Xia, Y. *Nano Lett.* **2005**, *5*, 2058–2062.
(86) Guo, S.; Dong, S.; Wang, E. *J. Phys. Chem. C* **2009**, *113*, 5485–5492.
(87) Shukla, A. K.; Neergat, M.; Bera, P.; Jayaram, V.; Hegde, M. S. *J. Electroanal. Chem.* **2001**, *504*, 111–119.
(88) Risbud, A. S.; Snedeker, L. P.; Elcombe, M. M.; Cheetham, A. K.; Seshadri, R. *Chem. Mater.* **2005**, *17*, 834–838.
(89) Jerkiewicz, G.; Vatankhah, G.; Lessard, J.; Soriaga, M. P.; Park, Y.-S. *Electrochim. Acta* **2003**, *49*, 1451–1459.
(90) Vetter, K. J.; Schultze, J. W. *J. Electroanal. Chem. Interfacial Electrochem.* **1972**, *34*, 141–158.
(91) Ahmad, M.; Pan, C.; Gan, L.; Nawaz, Z.; Zhu, J. *J. Phys. Chem. C* **2010**, *114*, 243–250.
(92) Schumacher, L. C.; Holzhueter, I. B.; Hill, I. R.; Dignam, M. J. *Electrochim. Acta* **1990**, *35* (6), 975–84.
(93) Dong, Z.; Fu, Y.; Han, Q.; Xu, Y.; Zhang, H. *J. Phys. Chem. C* **2007**, *111* (50), 18475–18478.
(94) Langell, M. A.; Anderson, M. D.; Carson, G. A.; Peng, L.; Smith, S. *Phys. Rev. B* **1999**, *59*, 4791–4798.
(95) Gulino, A.; Fragala, I. *Inorg. Chim. Acta* **2005**, *358*, 4466–4472.
(96) Pourbaix, M. *Atlas of electrochemical equilibria in aqueous solutions*; Pergamon: London, 1966; pp 322−329.
(97) Lichusina, S.; Chodosovskaja, A.; Selskis, A.; Leinartas, K.; Miecinskas, O.; Juzeliunas, E. *Chemija* **2008**, *19*, 7–15.
(98) Barbero, C.; Planes, F. A.; Miras, M. C. *Electrochem. Commun.* **2001**, *3*, 113–116.
(99) Perez, J.; Gonzalez, E. R.; Ticianelli, E. A. *Electrochim. Acta* **1998**, *44*, 1329–1339.
(100) Mayrhofer, K. J. J.; K., H.; Viktorija, J.; Arenz, M. *J. Am. Chem. Soc.* **2009**, *131*, 16348–16349.
(101) Duong, H. T.; Rigsby, M. A.; Zhou, W.-P.; Wieckowski, A. *J. Phys. Chem. C* **2007**, *111*, 13460–13465.
(102) Tejos, M.; Schrebler, R.; Diaz, F. R.; del Valle, M. A. *Thin Solid Films* **2002**, *409*, 172–177.
(103) Markovic, N. M.; Sarraf, S. T.; Gasteiger, H. A.; Ross, J. P. N. *J. Chem. Soc., Faraday Trans.* **1996**, *92*, 3719–3725.
(104) Kim, S.-H.; Maeng, J.-T.; Choi, C.-J.; Leem, J. H.; Han, M. S.; Seong, T.-Y. *Electrochem. Solid-State Lett.* **2005**, *8*, G167–G169.
(105) Pettersen, S. V.; Grande, A. P.; Tybell, T.; Riechert, H.; Averbeck, R.; Grepstad, J. K. *Semicond. Sci. Technol.* **2007**, *22*, 186–193.
(106) Macpherson, J. V.; Gueneau de Mussy, J.-P.; Delplancke, J.-L. *J. Electrochem. Soc.* **2002**, *149*, B306–B313.